

## An Efficient IWOLRS Control Technique of Brushless DC Motor for Torque Ripple Minimization

P. Rajesh\*

Department of Electrical and Electronics Engineering, Anna University, Chennai, Tamilnadu, India

Francis H. Shajin

Department of Electronics and Communication Engineering, Anna University, Chennai, Tamilnadu, India

G. Kodeeswara Kumaran

Department of Electrical and Electronics Engineering, M. S. Ramaiah Institute of Technology, Bangalore, India

\* Corresponding author. E-mail: rajeshkannan.mt@gmail.com      DOI: 10.14416/j.asep.2021.10.004

Received: 3 June 2021; Revised: 30 July 2021; Accepted: 25 August 2021; Published online: 11 October 2021

© 2022 King Mongkut's University of Technology North Bangkok. All Rights Reserved.

### Abstract

This manuscript proposes an improved DC-DC converter framework using a hybrid control algorithm for minimizing brushless DC motor (BLDC) torque ripple (TR). At first, the modeling of the brushless DC motor is intended by an enhanced Cuk converter (ECC). The function and performance of the Cuk converter are updated using the application of switched inductor. The control system integrates two control loops, as speed and torque control loop, which is employed to improve BLDC performance. Therefore, the Invasive Weed Optimization (IWO) and Local Random Search (LRS) are proposed to enhance control loop operations. In the IWO algorithm, the LRS approach is used as a part of the dispersion process to build up the course of action to find precision. This manuscript explores the IWO-LRS algorithm for limiting BLDC motor speed and torque error. Nevertheless, the exit from the proposed approach is subjected to the speed and torque controller input. The optimal gain parameters have been worked out to update the controller operation through the aid of necessary goal functions. The proposed controller topology is activated in MATLAB/Simulink site, and the performance is evaluated using other existing methods, like Particle Swarm Optimization (PSO), Bacterial Foraging (BF) algorithm.

**Keywords:** IWO, LRS, PSO, BLDC, Torque ripples, Speed, Current

### 1 Introduction

Today, there is a growing trend for utilizing BLDC instead of a brushed DC motor (BDC). BLDC motors contain certain benefits over the typical BDC and induction motors. These benefits are 1) better speed vs. torque properties, 2) higher dynamic response, 3) higher proficiency-lengthy operating life, 4) muted operation and 5) maximal speed range. Moreover, brushless DC motors are dependable, simple to control, inexpensive [1], [2]. The BLDC motor is the category of synchronous motor because the magnetic field

created through the stator and the rotor rotates at a similar frequency [3]. In general, the BLDC motor consists of permanent magnet rotor and 3 stator coils. At every control point, two of three coils are utilized for creating a magnetic field, when the floating coil induces an electro motive force (EMF) and returns that produced current to a controller [4]–[6].

Speed control is a significant feature in the brushless direct current motor drive for speed accuracy with position control uses [2]. The velocity response contains large overshoots under unstable periods and high fluctuations in steady-state periods. [7], [8] In

conventional speed control mode, the BLDC dual-loop speed control system is broadly employed at auto motive electronics, home appliances, etc., [9], [10]. The torque ripple under BLDC motor controls its used on higher accuracy drive scheme. The TR on the brushless DC motor can be caused by the number of actors, like commutation torque ripple. Therefore, it is important to suppress the commutation torque ripple to reduce the ripple of the BLOCM pair [11]. The torque consists of toothed, reluctance, and mutual torque and cogging torque with stator grooves [12]–[15]. Moreover, the reluctance of the torque is caused by a variation in phase inductance depending on the condition, and the mutual torque is generated through mutual coupling in the middle of the stator winding current and magnetic rotor [16]. In these motors, to diminish torque ripples, a trapezoidal back EMF is required. This is obtained by using concentrated winding, skewing the stator slots through a slotted passage. Therefore, a competent controller is necessary to diminish harmonics on input voltage to the motor.

The BLDC motor drive design includes complex process like modeling, selection of control unit, and simulation with stunning parameters. Nowadays, different sophisticated control units have been presented for brushless DC motor speed control design [17]. Several models are suggested to suppress the torque ripple via, phase change overlap model, the hysteresis current model, pulse width modulation model, current forecast control model, direct torque control. However, such models unavoidably have the issues of under/overcompensation, which is affecting the torque ripple suppression effect. The rotor speed, including position information, is required for the most brushless DC control methods [18]. The speed controller depending on Propotional Integral (PI), is activated for Brushless DC motor, other than the controller has created huge configuration time, increased time, oscillations under-speed response. Here, the least-squares random model, Genetic Algorithm (GA), PSO, Neural Network (NN), enhanced gradient decent approach is considered [19], [20].

Several research works were existed in the literature depending on the reduction of BLDC motor torque ripple using different processes and angles. Here, a part of them are reviewed.

Shi *et al.* [20] have shown a compensatory approach in combination using sensor BLDC or sensorless drive system for modifying that switching

moment of 2 half time frames over 60 °C lead time. Singh *et al.* [21] presented a power factor depending on the BLDC converter fed to Luo without a bridge. Kumar and Singh [9] have deemed the transmission of brushless DC motors powered by photovoltaic energy to the water pump. The DC-DC Cukconverter was utilized to function using the SPV group at the most extreme power. The initial BLDC motor current was restricted to the ideal state and the determination of the control parameters, irritation with recurrence.

Jiang *et al.* [22] established a novel control method for BLDC using compression loading. Chen *et al.* [23] established a new commutation evaluation technique for BLDCM depending on coordinate transformation theory and control of three-phase AC motor. In a two-phase stationary framework employing Clark transformation, the BLDCM model was acquired during the switching interval. To suppress the ripple of commutation torque, commutation control techniques and shortening of commutation time were determined.

Ge *et al.* [24] presented a conventional staggered tilt method to reduce gear torque at IPM machines. Bist and Singh [25] introduced a step-skewing rotor to optimum skew angles including a step-skewing rotor to non-equal pitch lengths. Here, to compensate three-dimensional effect were the two improved methods and minimize residual gear torque. Periasamy and Umayal [26] have portrayed the Power Factor Corrected Single-Ended Primary Inductor Converter (PFC-SEPIC) based voltage fed closed-loop full-bridge series resonant induction heating system for household induction heating applications.

Torque ripples are produced during electronic power commutation, maximal switch power devices frequency, stator fault, connected control system. In addition, the motor input supply voltage consists of several components of harmonical so pulsating input current based on electronic commutation causes torque ripple. However, many techniques have been implemented to reduce torque undulation, such as SVPWM, non-sinusoidal back EMF, coordinate transformation theory. Through the use of three-phase inverters, the center bypass voltage of the capacitor fluctuates and suggests an offset that destroys the balance between motor phase currents. To overwhelm this challenge, an optimal torque control method using superior methodology is necessary. Hence, the manuscript of the improved control method is established to

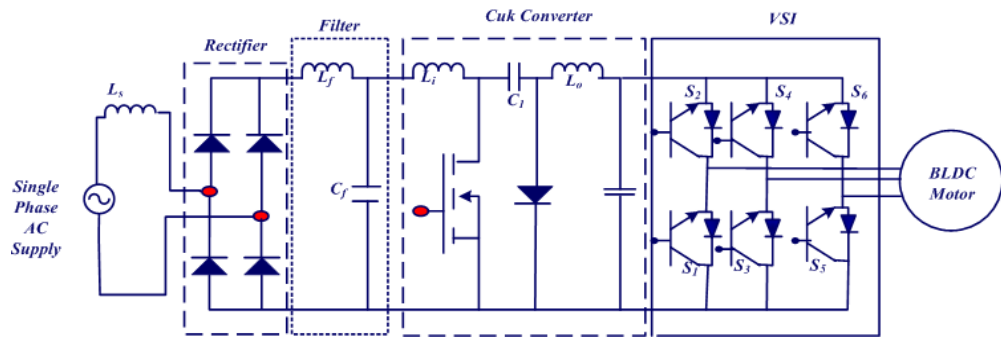


**Figure 1:** Dynamic framework of enhanced Cuk converter using BLDC motor.

resolve the previous problems.

An improved DC-DC converter framework using a hybrid control algorithm for minimizing brushless DC motor (BLDC) torque ripple is presented in the proposed study. The main novelty of the proposed work is to acquire the entire optimal solution, and then the optimal solution is collected by the search agents. The proposed study is useful for solving the optimization problem. Here the proposed approach is the combination of Invasive Weed Optimization (IWO) and Local Random Search (LRS). In the IWO algorithm, the LRS approach is used as part of the dispersion process to build up the course of action to find precision. The essential goal of the work is to limit the BLDC motor speed and torque error. The proposed method is activated in MATLAB/Simulink site, and the performance is examined with existing methods, viz PSO, BF algorithm. Accuracy, specificity, recall, and precision of proposed and existing methods with 50 and 100 trails, and RMSE, MAPE, and MBE with 50 and 100 trails are also analyzed. The accuracy, specificity, recall and precision of the proposed technique with 50 trails are 0.98, 0.96, 1.60, and 0.97, with 100 trails are 0.96, 0.93, 0.87, and 0.99.

## 2 Materials and Methods

Figure 1 portrays the dynamic drive system of the brushless direct current motor. This framework contains a BLDC motor, voltage source inverter, enhanced converter, DC filter, DBR, and an AC voltage source. The BLDC motor is linked edusing VSI at the three phases a, b, c, and the back EMF denoted  $e^a$ ,  $e^b$ ,  $e^c$  [27].

The measurement phase voltage regarding neutral point n. These are intended to model part of the

BLDC waste land assumed from the phase I process, i.e., the modeling process. At first, the AC input is provided with the DBR circuit, and then the DC filter circuit is passed. The enhanced converter is generated the VSI optimal control pulses. Rely on VSI, optimally controlled BLDC motor, and analyzed its performances. In this regard, the article proposes the invasive weed optimization algorithm (IWO) with local random search (LRS) to control speed and torque. This process is denoted as step II process, that is, the control method. The detailed evaluation model and control are explained in the following section.

### 2.1 Phase-I: Modeling process

Here, Figure 3 illustrates the modeling part of the BDC motor with the equivalent circuit. The speed control of the motor is employed high frequency PWM pulses are used the maximal loss of switch at 6 solid-state switches of voltage source inverter owing to maximal-frequency pulse width modulation signals. An improved Cuk converter has been employed after the diode bridge rectifier (DBR), a to recover the PQ and accomplish an integrity power component on the distribution framework. However, the voltage, including current stress on the PFC switch converter are increased in DICM as CICM, thus optimizing for lesser power consumption. After that, the Cuk converter is selected to decrease the cost of the framework to their application to lesser-control. It provides normal AC supply input and switches DC supply. The diode bridge rectifier has been employed to redress the input voltage of AC to DC that provided with boost segment. Among the switch ON-time, current flows through the rectifier diodes together with the ignition switch. Normally, the working principles

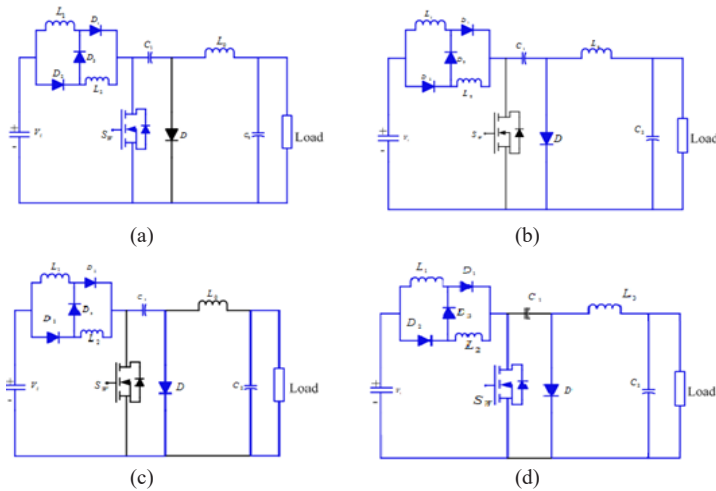


**Figure 2:** Operation of ECC under CCM (a), (b) DICM (c) DCVM (d).

of DC and VSI filters are earlier named and described in documents [28], [29]. The improved structure of the Cuk converter and operating performances are involved below:

### 2.1.1 Enhanced Cuk converter

The proposed non-isolated enhanced Cuk converter (ECC) contains switched inductor, here 2 capacitances are considered (i) switch (ii) diode. In inverting converter, the performance voltage implies -ve depending on information voltage [30]. The switched inductor realizes through a switch and a steering diode [31], which portrays in Figure 2.

When the active switch turn on, stage two inductors have been charged in parallel at a similar energy level. When active switches turn off stage, they have been discharged in series. The 2 inductors  $L_1$  and  $L_2$  are employed to individually change the input voltage source ( $V_i$ ), including performance voltage source ( $C_0$ ) at current sources. This change is significant in light of the fact, which capacitance was specifically connected with voltage source; the current would be limited only by parasitic resistance, which would cause a great vitality disgrace. The operation of ECC has four different techniques of CCM and DCM. Figure 2 (i) (a) and (b) displays the Cuk converter function at 2 different switching period intervals at CCM operation mode. The ECC function at two switching intervals on DICM and DCVM operation is described in

Figure 2 (i) (c and d). From Figure 2 (ii), the associated waveforms at the whole switching period have been evaluated. Figure 2 (ii) (a) shows that associated waveforms at the whole switching period at CCM operation mode are represented.

At CCM implementation of current under switched inductor ( $L_1$  and  $L_0$ ), voltage under the middle of capacitance  $C_1$  remains continuous at switching period [32]. At mode 1, while switch ( $S_w$ ) denotes turned ON, switched inductors save energy when capacitance ( $C_1$ ) is discharged during switch ( $S_w$ ) transmit their energy with DC-link capacitance ( $C_2$ ). At mode 2, while switch ( $S_w$ ) is turned OFF, energy stored is totally discharged with DCM operation. Amid this interim, no energy denotes left at input switched inductor and proves the current turn into zero. In addition, inductor  $L_0$  functions at continuous conductions, conveying its energy with dc-link capacitance ( $C_2$ ) individually. The enhanced Cuk switched inductor is exchanged to intermediary capacitance ( $C_1$ ) by a diode (D) until the converter is worked and examined their performances in the paper. Arithmetical modeling of brushless DC motor is specified at the given segment.

Figure 2(b) depicts the circuit diagram. Here, switch  $S_w$  is in the ON stage. Here,  $L_1$  charges, but  $L_2$  discharges during this period. The stored energy in  $L_2$  transfers to  $C_2$ , then it is charged. Moreover, by  $C_1$ ,  $S_w$ ,  $L_1$ ,  $L_2$ , load, the capacitor  $C_1$  is discharged, so transfer the saved energy at capacitor to the load. Consider the load current is steady, then flows in -ve direction.

Figure 2(c) depicts the circuit diagram. Here, both switches  $S_w$  are in the OFF stage. The inductors  $L_1$  and  $L_2$  are discharging during this time, then saved energy transmits to capacitors  $C_1$  and  $C_2$ . Then  $C_1$  starts charging. While,  $L_1$  and  $L_2$  inductors are discharged and transfers their energy to load represented in Figure (4).

Figure 2(c) portrays the equivalent circuit, here switch  $S_w$  is OFF state. On observing this Figure,  $L_2$  charges, but  $L_1$  discharges during this period. The saved energy on  $L_1$  transmits to  $C_1$ , also it continues to charge. The capacitor  $C_2$  discharges via  $C_2, S_w, L_2$ , load. Therefore, the stored energy is transferred from the capacitor to the load.

The operation is as same as that of mode 2.  $\Delta I = \Delta I_{L1} - \Delta I_{L2} = 0$ . At one-half cycle, when the switch is ON, the related inductor is charged, but another inductor is discharged, so the current ripple is cancelled. When Mode -1, Capacitor  $C_1$  works as the primary means of saving with transferring energy from the input to the output. Average inductor voltages  $V_{L1}$  and  $V_{L1}$  are over a period that implies zero under a constant level.

### 2.1.2 BLDC motor

The brushless DC motor mathematical model is plotted for speed and torque control analysis [33], [34]. To electro-mechanical systems small-signal analysis, the mode of average-value is PMSM along non-sinusoidal and brushless DC with trapezoidal back EMF. Figure 3 demonstrates that the equivalent circuit of the brushless DC motor is separated for every phase.

The electric dynamics of the brushless DC motor is composed up of accompanying voltage condition (1).

$$\delta_{abc}^s = \frac{d}{dt} \cdot (FL_{abc}^s) + \gamma^s \cdot \psi_{abc}^s \quad (1)$$

where  $\gamma^s$  represents stator resistance,  $\delta$  represents the stator voltage,  $\psi$  denotes stator current,  $FL$  denotes flux linkage provided at vectors like  $F_{abc}^s = [F_{ab}, F_{bc}, F_{cs}]^T$ ,  $F$  indicates stator voltage regarding with motor winding neutral point, flux linkage. Stator resistance array calculated in the situation (2).

$$\gamma^s = \text{diag}[\gamma^s, \gamma^s, \gamma^s] \quad (2)$$

The electromagnetic torque created at the attendance of back-EMF harmonics is categorized as

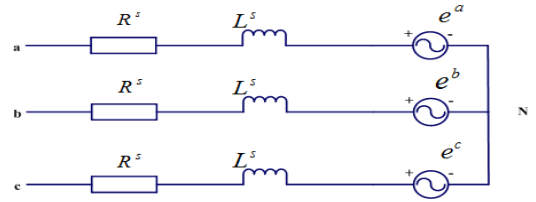


Figure 3: Equivalent circuit for each motor phase.

below condition (3).

$$\eta^e = \sum_{n=1}^{\infty} (2n-1) \cdot k_{2n-1} \cdot \begin{bmatrix} \psi_a^s \\ \psi_b^s \\ \psi_c^s \end{bmatrix} \cdot \begin{bmatrix} \cos(\theta^\gamma \cdot (2n-1)) \\ \cos\left((2n-1) \cdot \left(\theta^\gamma - \frac{2x}{3}\right)\right) \\ \cos\left((2n-1) \cdot \left(\theta^\gamma + \frac{2x}{3}\right)\right) \end{bmatrix} \cdot \left(\frac{p}{2} \cdot FL_m\right) \quad (3)$$

Where  $\eta^e$  represents the electromagnetic torque at the attendance of back-EMF. EMF phase voltages may be calculated in stator terminals while the machine is rotated to a primary mover and terminal is open circuit. Using condition (2) to (3) it is determined as Equation (4),

$$e_{abc}^s = \sum_{n=1}^{\infty} (2n-1) \cdot k_{2n-1} \cdot \begin{bmatrix} \cos(\theta^\gamma \cdot (2n-1)) \\ \cos\left((2n-1) \cdot \left(\theta^\gamma - \frac{2x}{3}\right)\right) \\ \cos\left((2n-1) \cdot \left(\theta^\gamma + \frac{2x}{3}\right)\right) \end{bmatrix} \cdot (\omega^\gamma \cdot FL_m) \quad (4)$$

If the back EMF motor consists of three harmonics, the stator neutral point voltage and -ve DC bus may last to three harmonics. The dynamic mechanical condition of motor speed Equation (5) is calculated.

$$\frac{d}{dt} \cdot (\phi^\gamma) = \left(\frac{P}{2j}\right) \cdot (\eta^e - \eta^m) \quad (5)$$

Where  $\frac{d}{dt} \cdot (\chi^\gamma)$  represents that electric angular speed of rotor regarding with  $t, j$  represents combined moment of load and inertia of the rotor,  $p$  implies magnetic pole count,  $\eta^m$  specifies joint mechanic torque. At first, the normal and speed reference is approximated from speed estimation.

### 2.1.3 CUK converter

This is a basic dc-dc converter, same as a buck-boost

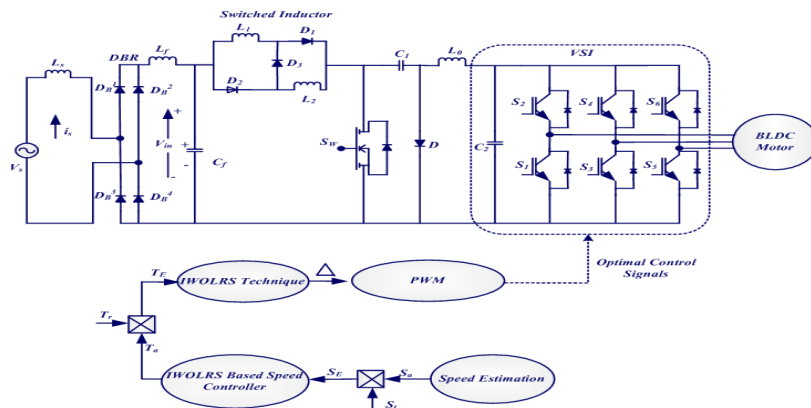


**Figure 4:** Control framework of BLDC motor based on proposed enhanced Cuk converter.

converter, and the output voltage polarity indicates negative. Here, the energy transfer from input to output through the capacitor. The converter has a pair of inductors with capacitors. The direct current connection voltage has to be set 4 times the back EMF during commutation interval. So, an immediate increase of dc connection voltage is essential when commutation according to the analysis of mathematical model. The CUK converter is appropriate to such requirements, making use of the topological advantages of the converter. Due to the negative polarity of the output voltage to the converter depending on the input voltage source negative terminal, there is a sudden increase at the 3 phase full-bridge inverter input voltage when turning on the auxiliary switch. The stator transmission interval is identified whenever there is a change in the Hall sensor output signals, and then the transmission interval end is determined when the current is zero in the outgoing phase (transmission phase). The auxiliary switch turns ON when this interval. The figure displays the instant, here phase b turns OFF, whereas phase c turns ON. The auxiliary switch turns ON for every 60 electrical deg because there are 6 commutation steps for a cycle of phase back EMF. The dc-dc converter is worked in 2 different modes of operation, which are regulated through the auxiliary switch. At 2 phase conduction period, the switch is turned off, and the diode is conducted with 3 phase inverter input voltage. It is mentioned that in traditional closed-loop speed control of BLDC drive, the dc connection voltage has been managed stable, also the speed is regulated by utilizing pulse width modulation to inverter switches which creates the loss of switching. In a DC-DC

converter fed BLDC drive, the pulse width modulation does not need for the speed control of the BLDC motor. The control strategy of the BLDC motor is described in the following segment.

## 2.2 Phase-II: Controlling process

Here, the control strategy of the brushless direct current motor is analyzed. This manuscript proposes a novel topology and the control strategy based on the IWO based LRS method. The mathematical model is formulated using the consideration of an improved Cuk converter. Figure 4 denotes the control arrangement of the proposed method. Here, the dynamic characteristics of the BLDC motor are analyzed. The presented method depends on the PI controller is generated for regulating speed with torque of the brushless DC motor. When a three-phase supply is provided to the DBR input, signals are then passed with VSI, and the optimal pulses should be produced to regulate the brushless DC motor. In this regard, the voltage of the three-phase source ( $V_{sa}$ ,  $V_{sb}$  and  $V_{sc}$ ) is given to the input.

### 2.2.1 Speed controller

In a brushless DC motor, the speed evaluates using a speed evaluator. Then the error signal is passed via the proposed speed controller to regulate the speed with the generation of torque reference. This PI controller improvement depends on two parameters value,  $K_p$ ,  $K_i$ . Hence, it is necessary to modify two parameters depending on the specified application. At first, the PI output controller is denoted as Equation (6),

$$U = K_p e_s(t) + K_i \int e_s(t) dt \tag{6}$$

Depending on the process time, the fault signal is computed in control operation. Similarly, the output signal provides the IWO-LRS method. In the operation of the IWO-LRS method, the IWO process is executed, which is updated using the LRS method. The values of the corresponding gain parameters are also stored from the output of the proposed method. The output is applied to the PI controller and creates optimal torque. Then the optimized control signals of the proposed controller are specified as given below Equation (7),

$$\xi(U) = K_p' e_s(t) + K_i' \int e_s(t) dt \tag{7}$$

here  $e_s(t) = S_i - S_a$ .

### 2.2.2 Torque controller

Depending on the real and reference torque value, the torque error is calculated. Then torque error values are given from the proposed PI controller to acquire the optimum control pulse of VSI. For this process, get optimum torque values along with control signals of VSI using Equation (8);

$$\xi(\Delta) = K_p'' e_t(t) + K_i'' \int e_t(t) dt \tag{8}$$

Here  $e_t(t) = T_r - T_a$ . Depending on the previous equation, optimal torque value is arrived. Then the minimization of torque ripples has also arrived. To minimize torque ripple Equation (9),

$$\mathfrak{R}\rho = \frac{T_{\max} - T_{\min}}{T_{\max} + T_{\min}} \tag{9}$$

To evaluate the percentage of TR, the earlier values are multiplied by 100. The torque is given with input of the proposed method to generate optimal motor control pulse. At last, the optimized output voltage signal is realized using inverter control switching operation and BLDC motor control efficiency. The development of optimal control signals is formulated at below Equation (10).

$$D(t) = \begin{cases} \text{if } e(t) > TD; & \text{then } D(t) = T_{on}^{\max} \\ \text{if } e(t) < TD; & \text{then } D(t) = T_{off}^{\max} \end{cases} \tag{10}$$

Here  $TD$  refers to a threshold value;  $T_{on}$  and  $T_{off}$  are on and off switches period,  $D(t)$  refers to the operating duty cycle of inverter switch. The below section denotes a brief working process of the proposed system.

### 2.3 Invasive Weed Optimization

The IWO approach is numeric stochastic with a derivative-free optimizer. Initially introduced by Mehrabian and Lucas for continuous performance optimization. Rather than colonizing the behavior of weed plants, the IWO approach emphasizes 3 stages 1) reproduction, 2) spatial dispersal 3) competitive expulsion. Mostly weeds are involved in the reproduction stage in the IWO method. However, the fertility of various weeds is not identical. The quantity of seeds created by weed relies upon their fitness. Fitter weeds deliver a large number of seeds than lesser fitter weeds. The weed seeds have approximately scattered under search area including normal distribution, mean equivalent to zero, adaptive standard deviation [35]. After propagation, the seeds with weeds prefer the competition. In this work, the IWO approach is applied to get optimal mean error value employing speed, and torque motor is restricted. The error signals are initialized as well as randomly generated by the advantage parameters of the PI controller. The initial population for applying the IWO algorithm is the error values  $E_i$  that are calculated by the difference between two speed and torque values.

#### Step 1: Initialization of population

The initial number of weeds is generated randomly in the search space. Each weed in the initial population is the error value  $E_i$ . Further, each weed is associated with two values (seeds)  $e_x$  and  $e_y$ . The inputs are initialized via the following Equation (11).

$$\bar{E}_l = [E_1, E_2, E_3, \dots, E_n] \tag{11}$$

where  $n$ = total count of weeds,  $\bar{E}_l$  denotes  $\bar{E}_l = (e_x, e_y)$ . Based on the above equation, the inputs are initialized.

#### Step 2: Fitness evaluation

Before reproducing the weeds, it is necessary to pick up the weeds that contain the best fitness values among the population. To get the minimal error function and achieve the optimal pulses Equation (12),

$$\text{Fitness} = \min(E) \quad (12)$$

Here error can be represented as  $E$ . Based on the above equation, the best weeds are estimated, and select the remaining weeds for the initial reproduction.

### Step 3: Reproduction

Each weed in the population is allowed to reproduce based on the fitness value, i.e., minimum error value ( $E$ ). The generation of new seeds is decreased linearly to produce seeds with the best fitness. The reproduced seed look like Equation (13),

$$E_i = \left[ (e_{x1}, e_{y1}), (e_{x2}, e_{y2}), \dots, (e_{xn}, e_{yn}) \right] \quad (13)$$

The reproduction is carried out based on the better and most horrible fitness at population Equation (14).

$$E_n = E_{\min} + (E_{\max} - E_{\min}) \frac{f - f_{\min}}{f_{\max} - f_{\min}} \quad (14)$$

Where  $E_n$  is the number of seeds to obtained be weed,  $E_{\min}$  is the number of seeds around the weed to min fitness,  $E_{\max}$  represents seed number around the weed to max fitness,  $f$  is the fitness of the selected weed,  $f_{\min}$  is the min fitness at the population,  $f_{\max}$  represents max fitness in the population.

### Step 4: Dispersion

Reproduced seed is dispersed in search space in this step. In order to maintain the dispersion of seed, the mean used for the IWO algorithm is globally a zero mean. However, the standard deviation  $\sigma$  varies non-linearly during each iteration. The seeds with the best fitness are grouped, for the best-fit weeds for the next iteration of reproduction Equation (15).

$$sd_{iter} = \left( \frac{iter_{\max} - iter}{iter_{\max}^n} \right)^n (sd_{\max} - sd_{\min}) + sd_{\min} \quad (15)$$

here number of iteration as  $iter_{\max}$ , standard deviation at the present step as  $sd_{iter}$ , non-linear modulation index as  $iter_{\max}^n$ .

For the process, the LRS technique is applied to get the optimal reproduced seeds.

### Local Random Search Method

To further improve the update function of IWO, an LRS depending on the method is established below. The initial search solution uses  $SD_i$ , with a fitness function value  $F(sd)$ .

- Fix a maximal number of local search repetitions iterLRS and identify neighborhood function  $H$ .
- Originator and only neighboring solution  $SD_j \in H(SD_i)$ , when meet restrictions and compute alter at the value of fitness function.
- Recognize solution  $SD_j (SD_i \leftarrow SD_j)$  if  $\phi_{ij} > 0$
- If maximal repetition to local search does not arrive, the repetition count is maximized to unique, then the previous process is frequent as step 2. Alternative, return  $SD_i$ ,  $OF(sd)$  denotes optimal outcomes get to the LRS algorithm. To get the optimum best solution, the proposed IWO algorithm is worked.

Based on the LRS method, the best reproduced weeds are discovered and evaluated their fitness function. Then the competitive expulsion steps are carried out.

### Step 5: Competitive expulsion

Among the reproduced seeds, if a weed does not generate any offspring, it is removed from the population. Flowchart of established algorithm displayed in Figure 5. From the output of the IWO algorithm, the optimum maximize parameter is estimated under torque and speed error signals.

## 3 Results and Discussion

The IWO-LRS process is imitated using the BLDC motor, and also implemented in the MATLAB/Simulink platform. It is performed with six switches VSI powered BLDC motor. At first, the parameter of the BLDC motor is examined like stator back EMF, stator current, speed, and torque correspondingly. Then, the IWO-LRS is operated at a torque controller that provides optimal control pulses of VSI as BLDC motor control. To analyze the performance of established techniques, this is experienced under the two different cases. First, the parameters of the BLDC motor are checked for stator back emf, stator current, speed, and torque, respectively. Table 1 shows the BLDC motor and CUK converter parameters.

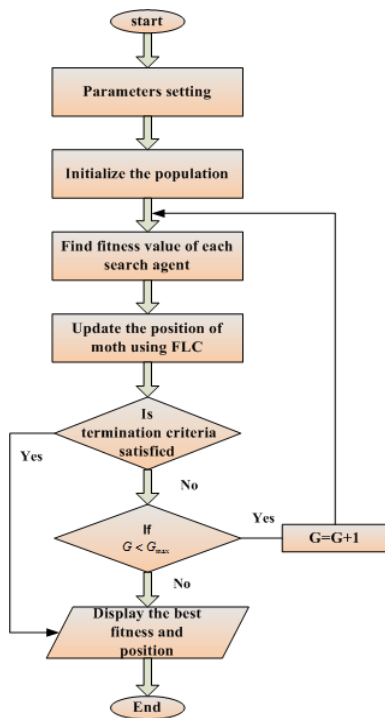


Figure 5: Flow chart of the IWO-LRS approach.

Table 1: BLDC motor and CUK converter parameters

BLDC Motor	
BLDC Parameters	Values
Stator phase resistance $R_s$ (ohm)	0.2
Stator phase inductance $L_s$ (H)	$8.5e-3$
Flux linkage	0.175
Back EMF flat area (degrees)	120
Inertia, viscousdamping, pole pairs, static friction [J(kg.m <sup>2</sup> ) F(N.m.s) p() Tf(N.m)]	[0.089,0.005,4]
CUK Converter	
Input voltage	12 V
Output voltage	30 V
Power rating	18 W
Inductor $L_1$	560 $\mu$ H
Inductor $L_2$	2.86 mH
Capacitor $C_1$	2 $\mu$ F
Capacitor $C_2$	470 $\mu$ F

**Case 1: Analysis of Steady-state**

**Case 2: Analysis of Dynamic state**

a) Analysis of Speed variant in the positive cycle (700 to 1500 rpm)

b) Analysis of Speed variation in the positive-negative cycle (1000 to -1000 rpm)

c) Analysis of Torque variation and Speed is constant

At steady-state analysis, the motor speed is fixed as the constant. However, dynamic analysis, speed, and torque are varied. The efficiency of the BLDC engine depends on the IWO-LRS technique denotes imitation of various techniques, like the PSO technique, BF method, and base model.

**Analysis of case 1**

Here, the static state evaluation of the BLDC motor is represented. Figure 6 suggests imitated state response of BLDC motor driven in 1000 rpm. Subplot 6 (a) and (b) shows the proposed method takes real, and reference speed at 1000 (rpm) calculates that output error speed increase time is 0 seconds together with adjustment process at 0.25 s.

Figure 7 displays that the analysis of current with proposed and existing methods. Subplot 7 (a) displays that the proposed method-based current output performance contains 0 seconds rise time of and settling time 0.25 s. Subplot 7 (b), (c), and (d) shows the existing methods such as PSO, BF, and normal based tuning process takes the 0 s rise time arrive settling time represents 0.3, 0.32, and 0.43 s. Figure 8 represents the EMF output performance evaluation to the IWO-LRS methodology. Here, BLDC motor output performance consists of increased time at 0 speeds (rpm) get 0.2 s to reach that stable condition, i.e., settling time.

**Analysis of case 2**

Here, the dynamic states are considered to analyze the BLDC motor, which is utilized the three states of analysis done using the proposed and existing methods. In this case, BLDC motor reference speed and torque vary, i.e., 700–1500 rpm, 1000 to -1000 rpm, and 3.3 to -3.3 Nm for case 1, case 2, case 3. The three states are described as below,

**Evaluation of Speed Variation in 700 to 1500 rpm**

Figure 8 represents Torque, back electro motive force, speed using input current. The motor speed has 0.05 s to reach the speed of reference following constant

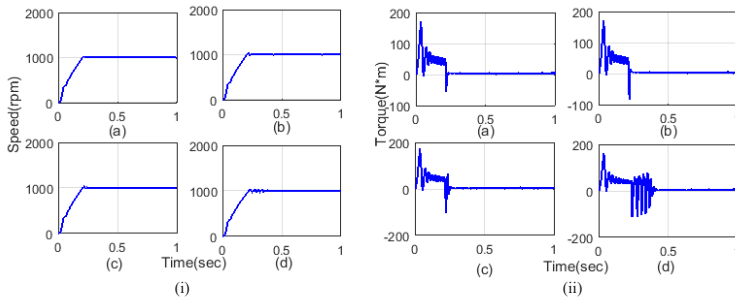


**Figure 6:** Analysis of (i) Speed (ii) Torque using (a) IWO-LRS method (b) PSO (c) BF and (d) Normal method.

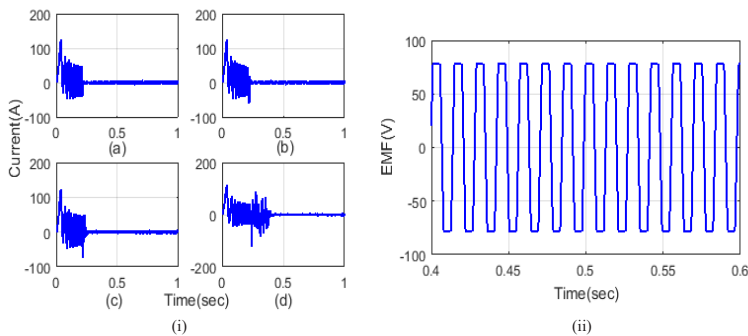


**Figure 7:** Analysis of (i) Current using (a) IWO-LRS method (b) PSO (c) BF and (d) Normal method (ii) Back EMF using the proposed method.

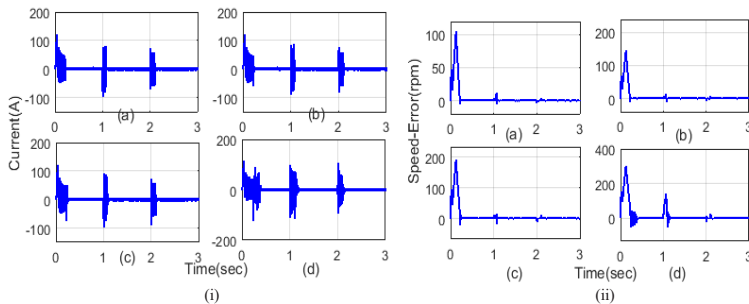


**Figure 8:** Analysis of (i) Current and (ii) Speed error using the (a) Proposed method (b) PSO (c) BF and (d) Normal method.

speed, only EMF become stable.

Figures 8 and 9 depicts the speed comparison of IWO-LRS and existing methods that clarify approximated speed of the established method is changed, i.e., the speed is varied into 1000 rpm at the time instant  $t = 0-1$  s. In addition, the speed is varied up to the high-level speed (i.e., 1500 rpm) in the time instant  $t = 1-2$  s. After the time instant  $t = 2$  s, the speed is reduced up

to 700 rpm. These figures variant time is focused and mention 0 to 3 s time period. The corresponding back EMF is also analyzed in Figure 10. The corresponding torque is analyzed in Figure 11.

In the IWO-LRS approach, the high torque eliminating in the waveform has been illustrated in Figure 11(b). From Figure 11(c), output performances of the current ripple, as a result, torque ripple of BLDC

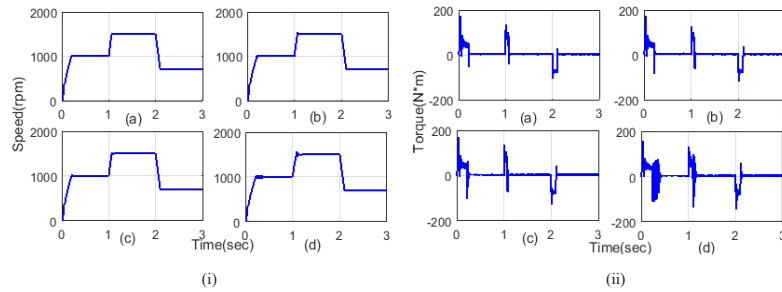


**Figure 9:** Analysis of (i) Speed and (ii) Torque using (a) proposed system (b) PSO (c) BF and (d) Normal method.

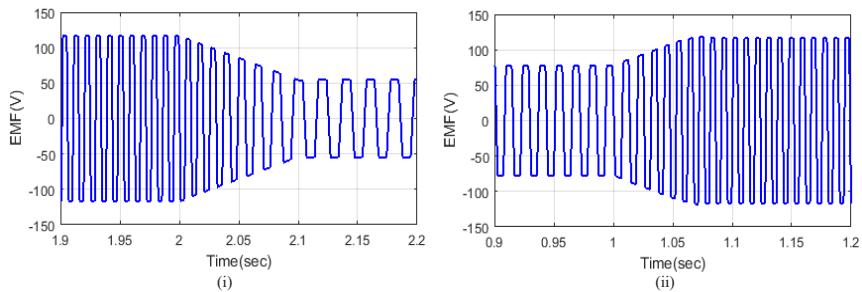


**Figure10:** Analysis of back EMF using the Speed Variation (i) 1500–700 and (ii) 1000–1500.

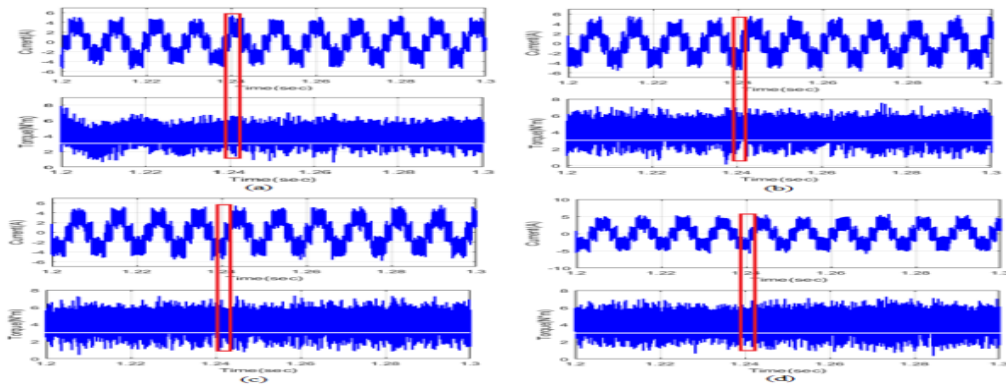


**Figure11:** Torque ripples analysis using (a) Normal (b) PSO (c) BF and (d) Proposed method.

motor has been diminished dramatically with the value of 1.3 of average load torque to implement PSO method. In BF, the high torque reduction in the waveform has been illustrated in Figure11.

**Evaluation of Speed Variation in 1000 to –1000 rpm**

Figures 12 and 13 display imitation outcomes and output of EMF phase orientation control system below the rated speed of 1000 rpm and –1000 rpm.

In dynamic state analysis, BLDC motor array

performances are evaluated as approximated Speed, Real Speed, Error Rate, Current, Torque, and back EMF, correspondingly. The reduction of torque waves is analyzed below the speed variant of 1000 to –1000 rpm depending on the above analysis. At first, operating speed was examined 1000 rpm.

Torque ripple analysis of established processes with existing is described in Figure 14. Here, the IWO-LRS algorithm is employed with minimized torque deviation likened to the PSO as well as BF algorithm attains 6.23, 8.47, and 4.12%.

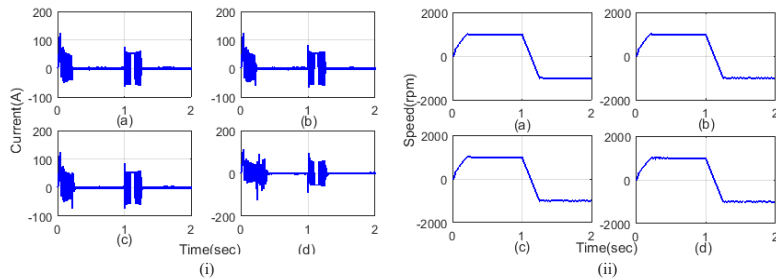


**Figure12:** Analysis of (i) Current and (ii) Speed using (a) Proposed method (b) PSO (c) BF and (d) Normal method.

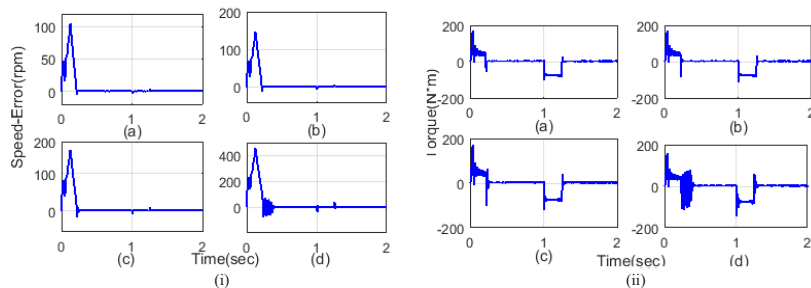


**Figure13:** Analysis of (i) Speed error and (ii) Torque using (a) Proposed system (b) PSO (c) BF and (d) Normal method.

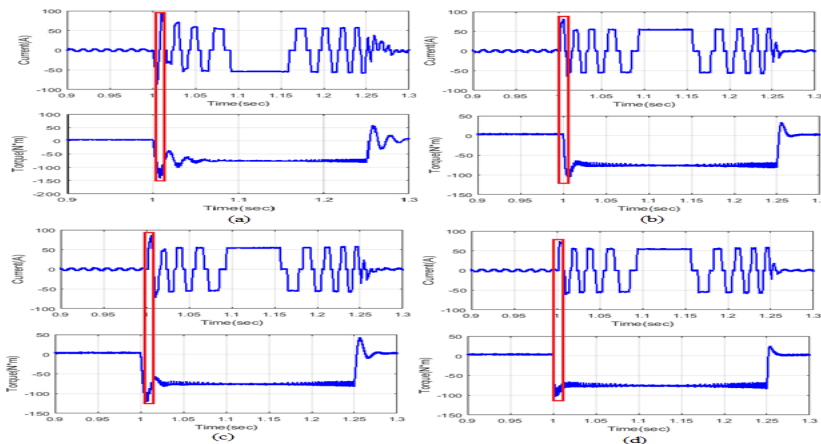


**Figure14:** Torque ripple analysis using (a) Normal (b) PSO (c) BF and (d) Proposed method.

### **Evaluation of Torque Variation in 3.3 to $-3.3$ and constant Speed**

Here, the IWO-LRS technique depends on minimizing TR in the BLDC motor. The IWO-LRS technique was utilized to attain the speed with torque control of BLDC motor. Figures 15 (i) and (ii) show that, the BLDC motor is optimized such as speed error and torque response for the proposed method, PSO, BF, and normal operation, has been analyzed. Figure 15 (i) and (ii) shows

that the output presentation employs established methodologies, which describe another technique. The IWO-LRS approach obtains stable rise time and the speed error to achieve 99.5 (rpm). The PSO and BF method-based speed error process takes 150 (rpm) and 190 (rpm). In Figure 15 (ii), the torque of the established technique and other methods vary from time to settlement process. In Figure 16 (i) and (ii) show that the analysis of speed and current in the proposed method and existing methods. Based on the proposed

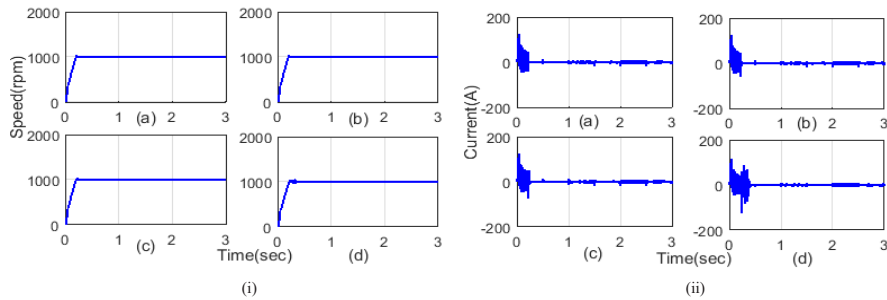


Figure 15: Analysis of (i) Speed and (ii) Current using (a) Proposed method (b) PSO (c) BF and (d) Normal method.

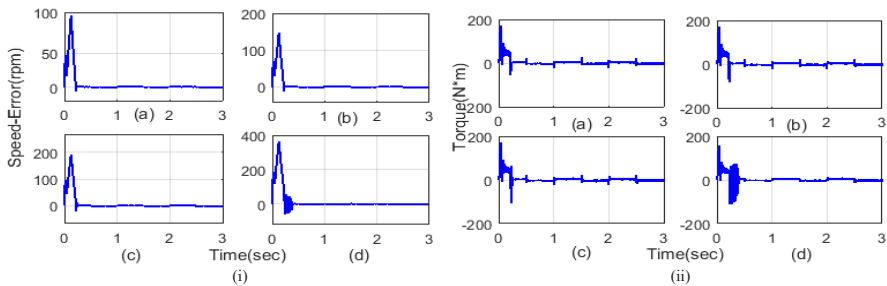


Figure 16: Analysis of (i) Speed error and (ii) Torque using (a) Proposed system (b) PSO (c) BF and (d) Normal method.

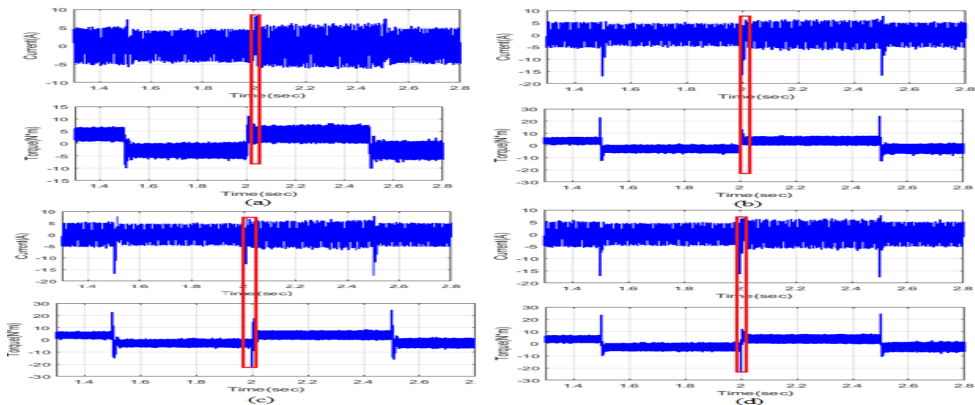


Figure 17: Torque ripples analysis using (a) Normal (b) PSO (c) BF and (d) Proposed method.

method, it contains a constant increase time and settling time of 1000 (rpm) seconds. Figure 16 (ii) displays current output performance of proposed and existing techniques.

Figure 17(a)–(d) displays the simulation outcomes for current waveforms and electromagnetic torque with and without comparing the IWO-LRS technique and existing methods decrease commutation torque, respectively.

Figure 17(a) illustrates the current ripple as a result, and the BLDC motor torque ripple has reduced

dramatically with a value of  $-2.5$  of average load torque implementing the PSO method. In Figure 17(b), the output ripples of the current ripple as a result torque ripple of the BLDC motor have reduced dramatically with value  $-12$  of average load torque. The IWO-LRS method of eliminating high torque in the waveform has been illustrated in Figure 17(c). Here, the current ripple causes BLDC motor torque ripple to be reduced sharply with value of  $-1.25$  average load torques implementing the established methodology. Figure 17(d) depicts the

current ripple as a result, motor torque ripple has reduced dramatically with value  $-12$  of average load torque implementing the BF method.

Table 2 tabulates the comparison of IWO-LRS performance using existing strategies for 50 and 100 assay counts, implying accuracy, specificity, recall, precision. At 50 trails, the IWO-LRS process achieves an accuracy of 0.98, a specificity of 0.96, a recall of 1.60, precision 0.97. In PSO, the ranges are 0.68, 0.42, 0.13, 0.39. In BF, the ranges are 0.72, 0.54, 0.36, 0.65. In 100 tracks, the IWO-LRS model achieves an accuracy of 0.96, a specificity of 0.93, a recovery of 0.87, and a precision of 0.99. At PSO it reaches the ranges of 0.55, 0.39, 0.66, 0.64. In BF, the ranges are 0.77, 0.57, 0.72, 0.63. Experimental results show that the IWO-LRS process is more efficient to than existing techniques.

**Table 2:** Performance comparison of IWO-LRS using existing for 50 and 100 count of trials

Performance Measures	50 Trails		
	PSO	BF	Proposed
Accuracy	0.68	0.72	0.98
Specificity	0.42	0.54	0.96
Recall	0.13	0.36	1.60
Precision	0.39	0.65	0.97
100 Trails			
Accuracy	0.55	0.77	0.96
Specificity	0.39	0.57	0.93
Recall	0.66	0.72	0.87
Precision	0.64	0.63	0.99

### 3.1 Statistical evaluation

Here, to compute error, the statistic measures via Root Mean Square Error (RMSE), Mean Absolute Percentage Error (MAPE), Mean Bias Error (MBE). The classification performance is analyzed in the proposed method subject to the RMSE error metric.

**Table 3:** Statistic comparison of IWO-LRS with existing methods for 50 and 100 count of trials

Metrics	50 Trails		
	PSO	BF	Proposed
RMSE	32.3	15.7	9.26
MAPE	17.5	8.5	0.95
MBE	8.2	6.1	1
100 Trails			
RMSE	24.8	29.2	7.38
MAPE	12.7	4.6	1.91
MBE	17.7	9.6	2.87

At the target value, a great alteration happens of mean the square error value is maximum. The calculation of the mean bias error is used for assessing the mean disturbance of the system. When the MBE value is negative, the diagnosis is underestimated. Also, the overall system performance is determined by the MAPE value. Table 3 tabulates the statistic analysis of the IWO-LRS method. Here, the IWO-LRS hybrid system is compared to existing techniques, namely PSO and BF, to assess overall performance. In solving the torque ripple minimization problem, the proposed approach is higher than the mentioned methods.

## 4 Conclusions

In this manuscript, the IWO-LRS hybrid process is used to examining the dynamic behaviors of the BLDC motor. The BLDC motor based on the IWO-LRS method is activated in MATLAB / Simulink site. Here, the modeling and control process is carried out with the help of the proposed system. The BLDC motor is provided by DBR, DC filter, updated Cuk converter, voltage source inverter devices. Cuk converter is formulated with the switched inductor for the modeling parts. On the controlling component, the speed with torque is regulated using the IWO-LRS method. Therefore, an improved proportional integral controller is proposed for regulating speed to lessen the BLDC motor torque ripple. BLDC motor is tested using a steady-state, including the dynamic state conditions. The above two conditions, the actual speed, the nominal speed, the error speed, the torque, the current, and the back electro motive force of the motor are deemed. The performance of the IWO-LRS method is likened to existing methods, like PSO and BF approaches. The feasibility of the IWO-LRS method is assessed as analysis, increased time, the settling time, and the overshoot time. In addition, torque ripples are resolved in terms of IWO-LRS with existing methods. At last, the experimental outcomes demonstrate that the proposed IWO-LRS system is more efficient than the other existing methods. Consequently, the torque ripple may almost diminish for its half value using the proposed drive model.

## References

- [1] S. Singh and B. Singh, "A voltage-controlled

- PFC Cuk converter-based PMBLDCM drive for air-conditioners,” *IEEE Transactions on Industry Applications*, vol. 48, no. 2, pp. 832–838, 2012.
- [2] J. Faiz, H. Nejadi-Koti, and Z. Valipour, “Comprehensive review on inter-turn fault indexes in permanent magnet motors,” *IET Electric Power Applications*, vol. 11, no.1, pp. 142–156, 2017.
- [3] F. Aghili, “Ripple suppression of BLDC motors with finite driver/amplifier bandwidth at high velocity,” *IEEE Transactions on Control Systems Technology*, vol. 19, no. 2, pp. 391–397, 2011.
- [4] S. Mythili, K. Thiyagarajah, P. Rajesh, and F. H. Shajin, “Ideal position and size selection of unified power flow controllers (UPFCs) to upgrade the dynamic stability of systems: An antlion optimiser and invasive weed optimisation algorithm,” *HKIE Transactions*, vol. 27, no. 1, pp. 25–37, 2020.
- [5] P. Rajesh and F. H. Shajin, “A multi-objective hybrid algorithm for planning electrical distribution system,” *International Information and Engineering Technology Association*, vol. 12, no. 4–5, pp. 377–387, 2020.
- [6] S. J. Park, H. W. Park, M. H. Lee, and F. Harashima, “A new approach for minimum-torque-ripple maximum-efficiency control of BLDC motor,” *IEEE Transactions on Industrial Electronics*, vol. 47, no. 1, pp. 109–114, 2000.
- [7] F. Aghili, M. Buehler, and J. Hollerbach, “Experimental characterization and quadratic programming-based control of brushless-motors,” *IEEE Transactions on Control Systems Technology*, vol. 11, no. 1, pp. 139–146, 2003.
- [8] H. S. Seol, D. W. Kang, H. W. Jun, J. Lim, and J. Lee, “Design of winding changeable BLDC motor considering demagnetization in winding change section,” *IEEE Transactions on Magnetics*, vol. 53, no. 11, pp. 1–5, 2017.
- [9] R. Kumar and B. Singh, “Solar PV powered BLDC motor drive for water pumping using Cuk converter,” *IET Electric Power Applications*, vol. 11, no. 2, pp. 222–232, 2017.
- [10] J. Fang, H. Li, and B. Han, “Torque ripple reduction in BLDC torque motor with nonideal back EMF,” *IEEE Transactions on Power Electronics*, vol. 27, no. 11, pp. 4630–4637, 2012.
- [11] H. E. A. Ibrahim, F. N. Hassan, and A. O. Shomer, “Optimal PID control of a brushless DC motor using PSO and BF techniques,” *Ain Shams Engineering Journal*, vol. 5, no. 2, pp. 391–398, 2014.
- [12] S. K. M. Niapour, M. Tabarraie, and M. R. Feyzi, “A new robust speed-sensorless control strategy for high-performance brushless DC motor drives with reduced torque ripple,” *Control Engineering Practice*, vol. 24, pp. 42–54, 2014.
- [13] H. Guzman, M. J. Duran, F. Barrero, B. Bogado, and S. Toral, “Speed control of five-phase induction motors with integrated open-phase fault operation using model-based predictive current control techniques,” *IEEE Transactions on Industrial Electronics*, vol. 61, no. 9, pp. 4474–4484, 2014.
- [14] M. Masmoudi, B. ElBadi, and A. Masmoudi, “Direct torque control of brushless DC motor drives with improved reliability,” *IEEE Transactions on Industry Applications*, vol. 50, no. 6, pp. 3744–3753, 2013.
- [15] T. Sheng, X. Wang, J. Zhang, and Z. Deng, “Torque-ripple mitigation for brushless DC machine drive system using one-cycle average torque control,” *IEEE Transactions on Industrial Electronics*, vol. 62, no. 4, pp. 2114–2122, 2015.
- [16] T. Shi, Y. Guo, P. Song, and C. Xia, “A new approach of minimizing commutation torque ripple for brushless DC motor based on DC–DC converter,” *IEEE Transactions on Industrial Electronics*, vol. 57, no.10, pp. 3483–3490, 2010.
- [17] H. Lu, L. Zhang, and W. Qu, “A new torque control method for torque ripple minimization of BLDC motors with un-ideal back EMF,” *IEEE Transactions on Power Electronics*, vol. 23, no. 2, pp. 950–958, 2008.
- [18] C. Zhu, Z. Zeng, and R. Zhao, “Comprehensive analysis and reduction of torque ripples in three-phase four-switch inverter-fed PMSM drives using space vector pulse-width modulation,” *IEEE Transactions on Power Electronics*, vol. 3, no. 7, pp. 5411–5424, 2017.
- [19] Transpire Online, “A Novel Numerical Optimization Algorithm Inspired from Particles: Particle Swarm Optimization,” 2020. [Online]. Available: <https://transpireonline.blog/2019/07/03/a-novel-numerical-optimization-algorithm-inspired-from-particles-particle-swarm-optimization/>
- [20] T. Shi, Y. Cao, G. Jiang, X. Li, and C. Xia, “A torque control strategy for torque ripple reduction of brushless DC motor with nonideal

- back electromotive force,” *IEEE Transactions on Industrial Electronics*, vol. 64, no. 6, pp. 4423–4433, 2017.
- [21] B. Singh, V. Bist, A. Chandra, and K. Al-Haddad, “Power factor correction in bridgeless-luo converter-fed bldc motor drive,” *IEEE Transactions on Industry Applications*, vol. 51, no. 2, pp. 1179–1188, 2015.
- [22] W. Jiang, H. Huang, J. Wang, Y. Gao, and L. Wang, “Commutation analysis of brushless DC motor and reducing commutation torque ripple in the two-phase stationary frame,” *IEEE Transactions on Power Electronics*, vol. 32, no. 6, pp. 4675–4682, 2017.
- [23] W. Chen, Y. Liu, X. Li, T. Shi, and C. Xia, “A novel method of reducing commutation torque ripple for brushless DC motor based on Cuk converter,” *IEEE Transactions On Power Electronics*, vol. 32, no. 7, pp. 5497–5508, 2017, doi: 10.1109/tpe.2016.2613126.
- [24] X. Ge, Z. Zhu, G. Kemp, D. Moule, and C. Williams, “Optimal step-skew methods for cogging torque reduction accounting for three-dimensional effect of interior permanent magnet machines,” *IEEE Transactions on Energy Conversion*, vol. 32, no. 1, pp. 222–232, 2017, doi: 10.1109/tec.2016.2620476.
- [25] V. Bist and B. Singh, “Reduced sensor configuration of a power factor correction based single-ended primary inductance converter fed brushless DC motor drive,” *IET Power Electronics*, vol. 8, no. 9, pp. 1606–1615, 2015.
- [26] M. Periasamy and C. Umaya, “Improved time responses of PI FL controlled SEPIC converter-based series resonant inverter-fed induction heating system,” *International Journal of Power Electronics and Drive System (IJPEDS)*, vol. 9, no. 1, pp. 305–315, 2018.
- [27] B. N. Kommula and V. R. Kota, “An integrated converter topology for torque ripple minimization in BLDC motor using an ITSA technique,” *Journal of Ambient Intelligence and Humanized Computing*, Mar. 2021, doi: 10.1007/s12652-021-02986-4.
- [28] R. Foroozeshfar, H. Farzanehfard, and E. Adib, “New single-stage, single-switch, soft-switching three-phase SEPIC and Cuk-type power factor correction converters,” *IET Power Electronics*, vol. 7, no. 7, pp. 1878–1885, 2014.
- [29] B. Poorali, E. Adib, and H. Farzanehfard, “Soft-switching DC–DC Cuk converter operating in discontinuous-capacitor-voltage mode,” *IET Power Electronics*, vol. 10, no. 13, pp. 1679–1686, 2017.
- [30] A. Esmaili and H. Babazadeh, “A foreground self-calibration technique for high-resolution switched-current R-2R digital-to-analog converters,” *Circuits, Systems, Signal Processing*, vol. 39, no. 5, pp. 2307–2327, 2019.
- [31] T. Shi, X. Niu, W. Chen, and C. Xia, “Commutation torque ripple reduction of brushless DC motor in braking operation,” *IEEE Transactions on Power Electronics*, vol. 33, no. 2, pp. 1463–1475, 2018.
- [32] G. Jiang, C. Xia, W. Chen, T. Shi, X. Li, and Y. Cao, “Commutation torque ripple suppression strategy for brushless DC motors with a novel noninductive boost front end,” *IEEE Transactions on Power Electronics*, vol. 33, no. 5, pp. 4274–4284, 2018.
- [33] T. Velmurugan, S. Khara, S. Nandakumar, and B. Saravanan, “Seamless vertical handoff using invasive weed optimization (IWO) algorithm for heterogeneous wireless networks,” *Ain Shams Engineering Journal*, vol. 7, no. 1, pp. 101–111, 2016.
- [34] D. R. Prabha and T. Jayabarathi, “Optimal placement and sizing of multiple distributed generating units in distribution networks by invasive weed optimization algorithm,” *Ain Shams Engineering Journal*, vol. 7, no. 2, pp. 683–694, 2016.
- [35] Y. Wu, R. Jin, and X. Zhang, “Efficient and exact local search for random walk based top-k proximity query in large graphs,” *IEEE Transactions on Knowledge and Data Engineering*, vol. 28, no. 5, p. 116, 2016.